



Contents lists available at ScienceDirect

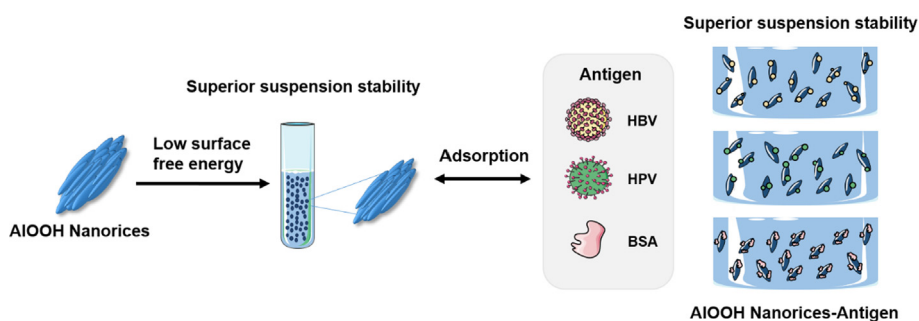
Journal of Colloid and Interface Science

journal homepage: www.elsevier.com/locate/jcis

Self-assembled aluminum oxyhydroxide nanorices with superior suspension stability for vaccine adjuvant

Shisheng Bi^{a,b,1}, Min Li^{a,b,1}, Zhihui Liang^{a,b,1}, Guangle Li^c, Ge Yu^{a,b}, Jiarui Zhang^{a,b}, Chen Chen^d, Cheng Yang^e, Changying Xue^d, Yi Y. Zuo^c, Bingbing Sun^{a,b,*}^aState Key Laboratory of Fine Chemicals, Dalian University of Technology, 2 Linggong Road, 116024 Dalian, China^bSchool of Chemical Engineering, Dalian University of Technology, 2 Linggong Road, 116024 Dalian, China^cDepartment of Mechanical Engineering, University of Hawaii at Manoa, Honolulu, HI 96822, United States^dSchool of Bioengineering, Dalian University of Technology, 2 Linggong Road, 116024 Dalian, China^eSchool of Chemistry, Dalian University of Technology, 2 Linggong Road, 116024 Dalian, China

GRAPHICAL ABSTRACT



ARTICLE INFO

Article history:

Received 1 April 2022

Revised 18 May 2022

Accepted 4 July 2022

Available online 11 July 2022

Keywords:

Vaccine adjuvant
 Aluminum oxyhydroxide
 Surface free energy
 Suspension stability

ABSTRACT

The suspension stability of aluminum-based adjuvant (Alum) plays an important role in determining the Alum-antigen interaction and vaccine efficacy. Inclusion of excipients has been shown to stabilize antigens in vaccine formulations. However, there is no mechanistic study to tune the characteristics of Alum for improved suspension stability. Herein, a library of self-assembled rice-shaped aluminum oxyhydroxide nanoadjuvants *i.e.*, nanorices (NRs), was synthesized through intrinsically controlled crystallization and atomic coupling-mediated aggregations. The NRs exhibited superior suspension stability in both water and a saline buffer. After adsorbing hepatitis B surface antigen (HBsAg) virus-like particles (VLPs), human papillomavirus virus (HPV) VLPs, or bovine serum albumin, NR-antigen complexes exhibited less sedimentation. Further mechanistic study demonstrated that the improved suspension stability was due to intraparticle aggregations that led to the reduction of the surface free energy. By using HBsAg in a murine vaccination model, NRs with higher aspect ratios elicited more potent humoral immune responses. Our study demonstrated that engineered control of particle aggregation provides a novel material design strategy to improve suspension stability for a diversity of biomedical applications.

© 2022 Elsevier Inc. All rights reserved.

* Corresponding author at: State Key Laboratory of Fine Chemicals, Dalian University of Technology, 2 Linggong Road, 116024 Dalian, China.

E-mail address: bingbingsun@dlut.edu.cn (B. Sun).

¹ These authors have equal contributions.

1. Introduction

Adjuvant is one of the major components in subunit and certain inactivated vaccines. Aluminum-based adjuvants (Alum) have

been widely used in pharmaceutical preparations due to their capability to induce humoral immunity [1–3]. When suspended in aqueous solutions for formulation, Alum tend to aggregate spontaneously [4,5]. When antigen is adsorbed to Alum, the adjuvant-antigen complexes are exposed to interfacial stress, which reduces the adjuvant's suspension stability, thus further promoting agglomeration, and resulting in compromised immune stimulating effects [6]. It is recommended that Alum-adjuvanted vaccines, e.g., Pevnar 13[®], Cervarix[®], Havrix[®], need to be homogenized before administration to avoid unwanted precipitations.

The suspension stability of the Alum-adjuvanted vaccines is affected by the presence of both adjuvant and antigen [7]. By using excipients to stabilize the antigen, the suspension and dispersion of vaccines can be improved [8]. However, the presence of excipients increases the complexity of the vaccine formulation, and the process of optimizing the formulation is usually tedious [9]. The adjuvant in formulation can be considered as inorganic nanoparticles (NPs) [10,11], and many studies have demonstrated that the intrinsic properties of NPs can affect the suspension stability. Based on the classical DLVO theory, the higher zeta potential leads to higher electrostatic repulsion, which could increase the suspension stability [12]. According to Stokes' law, the smaller particle size and suitable rheology can improve the suspension of NPs [13,14]. However, when the local concentration of NPs exceeds the critical coagulation concentration due to aggregation, they rapidly form large clusters and then precipitate [15,16]. Strategies including electrostatic repulsion and steric stabilization [17–19] have been proposed to improve the suspension state of NPs by adding either ionic [20] or nonionic stabilizers [21–23]. Nevertheless, stabilizers could alter the overall properties of NPs and only a very limited number of surfactants are permitted for use in biopharmaceutical formulations [24,25]. NPs with superior suspension properties have been synthesized without stabilizers [26,27]. For example, 2-devinyl-2-(1-hexyloxyethyl) pyrophosphorus compound (HPPH) nanosuspension was prepared to exhibit a better suspension stability due to the high zeta potential generated by deprotonation of the carboxyl group of HPPH molecules [28]. In addition, the formation of SnO₂-TiO₂ heterojunction *via* efficient interfacial charge transfer at particle-particle interface provided a stronger interparticle charge separation to avoid aggregation [29,30]. We therefore hypothesize that the intrinsic property of Alum could be engineered to avoid their agglomeration and optimize suspension.

It has been demonstrated that aluminum oxyhydroxide could be engineered to control their physicochemical properties [31–40]. In this article, a library of rice-shaped aluminum oxyhydroxide nanoadjuvants, *i.e.*, nanorices (NRs), with different aspect ratios was synthesized by the hydrothermal process. The intraparticle aggregations were formed through controlling the atomic interface coupling. As a result, engineered aggregation reduced the surface free energy of NRs and enhanced their suspension stability. After being formulated with model antigens, *e.g.*, hepatitis B surface antigen (HBsAg) virus-like particles (VLPs), human papillomavirus virus (HPV) VLPs, and bovine serum albumin (BSA), the NR-antigen complexes also exhibited improved suspension stability. In a mouse model, the NR-adjuvanted HBsAg vaccine induced enhanced antibody responses. This study provides novel insights into designing engineered adjuvants with superior suspension stability, and further ensures improved immunogenicity of vaccines.

2. Experimental section

2.1. Reagents and materials

Aluminum (III) nitrate nonahydrate [Al(NO₃)₃·9H₂O], urea were purchased from ShengGong (Shanghai, China). Fluorescein isothio-

cyanate isomer I (FITC) was purchased from Macklin (Shanghai, China). Lipopolysaccharide (LPS) and J774A.1 cells were purchased from Sigma (St. Louis, MO). The goat anti-mouse polyclonal secondary antibodies specific for total IgG, IgG₁, and IgG_{2c} were obtained from Abcam (Cambridge, British). Hepatitis B surface antigen (HBsAg) was kindly provided by NCPC Genetech Biotechnology Co., Ltd. (Shijiazhuang, China). Human papillomavirus (HPV) VLP type 18 was purchased from Zerun Biotechnology Co., Ltd. (Shanghai, China).

2.2. Synthesis of rice-shape aluminum oxyhydroxide nanoadjuvants (NRs)

In a typical synthesis of NRs, 0.9375 g of aluminum(III) nitrate nonahydrate [Al(NO₃)₃·9H₂O] and 0.3 g of urea were dissolved in 50 mL of deionized water to form a clear solution. After vigorous stirring for 10 min, the mixture was transferred into two 23-mL Teflon-lined stainless-steel autoclaves and kept at 180 °C in an oven for 45 min. Then, the autoclave was cooled in the air. The fresh precipitate was separated by centrifugation at 10,000 rpm for 10 min and washed sequentially with ethanol and deionized water for three cycles. For the NRs (NR 1, NR 2, NR 3 and NR 4), they were prepared with urea content at 0.30, 0.60, 0.90 and 1.95 g, respectively. For the FITC-labelled NRs, 10 mg of particles were suspended in 2 mL of dimethylformamide (DMF), then 0.4 μL of aminopropyltriethoxysilane (APTES) was added. After reacting at 25 °C for 4 h, nanoparticles were washed with DMF and re-suspended in DMF (1.5 mL). 150 μL of FITC (2 mg/mL in DMF) was added into the suspension and stirred at 1000 rpm for 30 min. The FITC-labeled nanoparticles were washed with ultrapure water for several times and re-suspended in ultrapure water at 10 mg/mL.

2.3. Characterization of NRs

The NRs were determined by transmission electron microscopy (TEM, JEOL JEM-1200EX) at an acceleration voltage of 120 kV. The hydrodynamic sizes and zeta potentials of NRs or NRs-antigen complexes in water and medium were measured by a dynamic light scattering instrument (DLS, Brookhaven, 90 plus PALS). The crystal structures of NRs were determined by a Philips X'pert X-ray diffraction (XRD, Rigaku D/Max 2400 type X-ray spectrometer) equipped with Cu K α radiation ($\lambda = 1.54178 \text{ \AA}$). Diffractograms were obtained when 2θ increased from 5° to 80°.

2.4. Determined the surface free energy of AlOOH nanoparticles

The determination of surface free energy of AlOOH nanoparticles was based on a maximum particle dispersion (MPD) method [41]. Briefly, a series of ethanol/water liquids which surface tensions ranging from 22 mJ/m² (for pure ethanol) to 72 mJ/m² (for pure water). AlOOHs were dispersed in different suspending liquids with the concentration of 1.0 mg/mL. After centrifugation at 2348 g for 4 min, the supernatants were collected and the absorbance at 400 nm was determined. The surface free energy was determined to be equal to the surface tension of the suspending liquids in which the AlOOH nanoparticles were dispersed maximumly.

2.5. Determination of adsorption of antigen by AlOOH nanoparticles

10 mM of MOPS buffer was prepared, and the pH of the buffer was adjusted to 7.4 with 0.1 M of NaOH. 0.5 mL of HBV protein working solution (50–200 μg/mL) and 0.5 mL of nanoparticle suspension in a desired concentration (150 μg Al/mL) were mixed in a microcentrifuge tube. The samples were allowed to equilibrate

with agitation for 30 min. The concentration of protein in the supernatant was measured by the micro bicinchoninic acid (BCA) protein assay kit (Oregon, USA). The Langmuir equation was used to describe adsorption in which the solute was adsorbed to form a monolayer. The Langmuir equations were fitted for the adsorption of HBV according to method described previously [42].

2.6. Animal vaccination

6-week female BALB/c mice were purchased from Dalian Medical University. Animals were housed under specific pathogen-free (SPF) conditions according to Dalian University of Technology guidelines for care and treatment of laboratory animals. Dalian University of Technology Animal Research Committee allowed our protocols. Before vaccination, HBsAg was pre-adsorbed to AIOOH nanorices in 0.9% saline buffer. Formulated vaccines, containing 2 μg of HBsAg and 111.10 μg of AIOOH in a total volume of 50 μL , were immunized mouse by muscle injection on day 0 and 21. The HBsAg immunized mice were used as control samples. The serum of vaccinated mice was collected on day 42, and the HBsAg-specific antibody titers were determined by ELISA. Briefly, ELISA plate was coated with 2 $\mu\text{g}/\text{mL}$ of HBsAg in 50 mM of carbonate buffer (pH 9.6) at 4 $^{\circ}\text{C}$ for 12 h. The unbound antigen was removed by using wash buffer (0.05% Tween 20 in PBS). Then the plate was blocked with 10% (v/v) FBS in PBS. A series of different dilutions of serum were added to the plate and incubated at 37 $^{\circ}\text{C}$ for 2 h. Then the plate was treated with 100 μL of HRP-

conjugated antibody (diluted 1:10,000) for 2 h. After the plate was washed by wash buffer, 100 $\mu\text{L}/\text{well}$ of TMB substrate was added and incubated for 10 min. Finally, the enzymatic reaction was stopped by adding 50 $\mu\text{L}/\text{well}$ of 1 M H_2SO_4 , and the OD 450 nm was measured. The endpoint titers were calculated as the maximum dilution multiple of the last dilution reaching a cut-off value, which was set to twice the mean optical density of a negative control [43,44].

2.7. Statistical analysis

All experiments were performed in triplicate, and the values were expressed as means \pm SD. Two-tailed Student's *t*-test was used to determine statistical significance for the difference between two sets of data.

3. Results and discussion

3.1. Synthesis and characterization of aluminum oxyhydroxide nanorice

A library of aluminum oxyhydroxide (AIOOH) nanoparticles was prepared using a hydrothermal method by controlling the molar ratio of $\text{Al}(\text{NO}_3)_3 \cdot 9\text{H}_2\text{O}$ (Al) to urea. Transmission electron microscopy (TEM) analysis showed that these particles all exhibited a rice shape (Fig. 1a). The aspect ratio of NRs was regulated by Al to urea ratio. With the increase of urea, the length of NRs

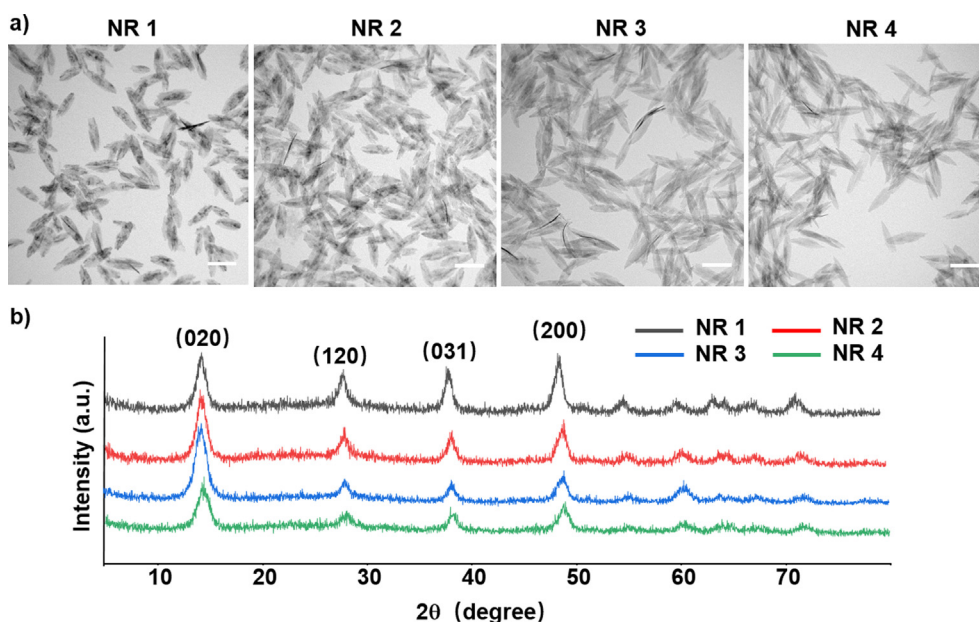


Fig. 1. (a) TEM analysis of NRs. Scale bar = 500 nm. (b) XRD analysis of NRs.

Table 1
Characterizations of NRs and Alhydrogel[®].

Sample ID	Length (nm)	Diameter (nm)	Aspect ratio	Hydrodynamic sizes in water (nm)	Poly-dispersity index	Zeta potentials in water (mV)	Surface hydroxyl content (mmol/g)	Specific surface area (m^2/g)
NR 1	528 \pm 22	147 \pm 07	3.51 \pm 0.24	275.65 \pm 2.93	0.14 \pm 0.03	50.31 \pm 1.68	0.062	59.54
NR 2	609 \pm 28	165 \pm 11	3.72 \pm 0.42	267.95 \pm 1.72	0.17 \pm 0.07	48.35 \pm 1.36	0.055	85.66
NR 3	754 \pm 43	175 \pm 19	4.37 \pm 0.60	268.97 \pm 8.55	0.16 \pm 0.04	49.92 \pm 1.11	0.043	118.73
NR 4	780 \pm 36	160 \pm 15	4.93 \pm 0.71	273.25 \pm 1.93	0.15 \pm 0.04	47.43 \pm 1.04	0.035	120.91
Alhydrogel [®]	45 \pm 9	7 \pm 1	6.01 \pm 0.92	258.83 \pm 4.95	0.23 \pm 0.01	21.84 \pm 1.72	N.D.	289.68

N.D. not detected.

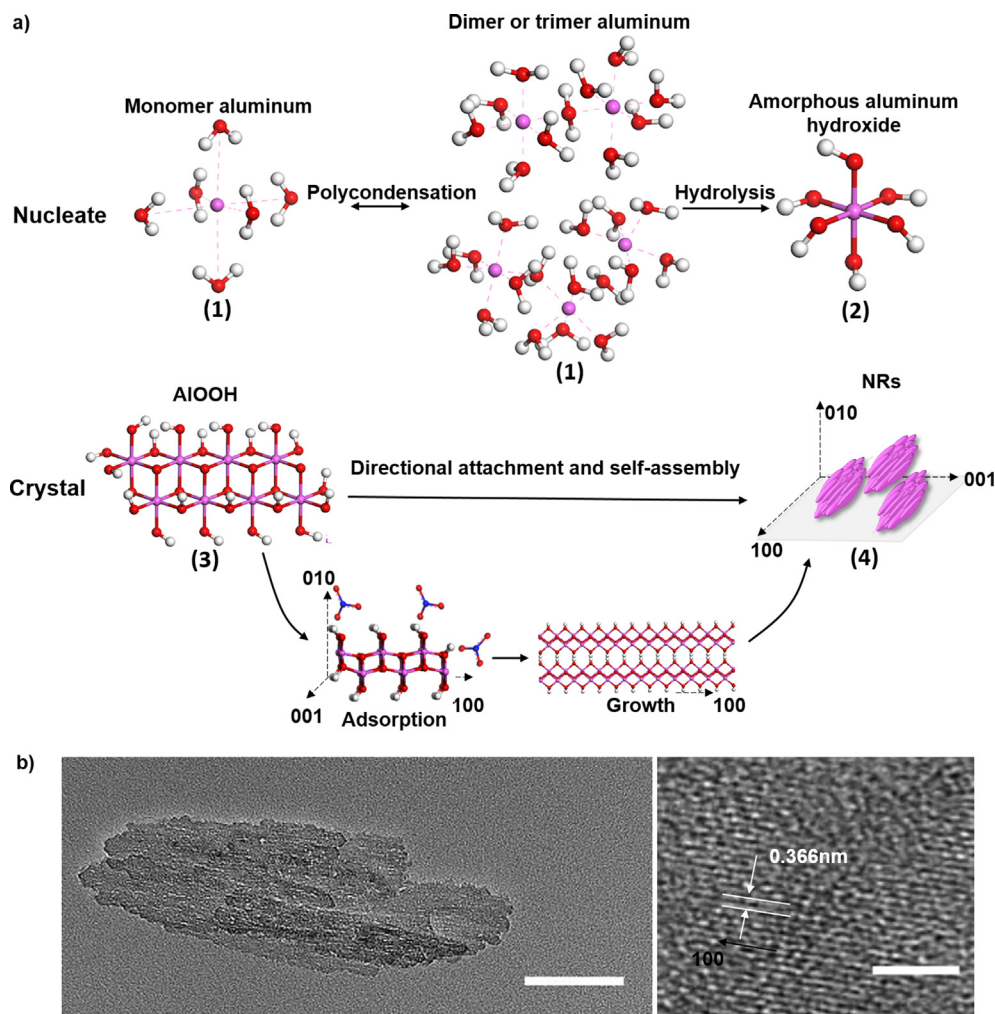


Fig. 2. (a) The formation mechanism of NRs. (b) High resolution Transmission Electron Microscopy (HRTEM) analysis of NR 1. The scale bars are 100 nm (left panel) and 2 nm (right panel), respectively. The corresponding (0 0 1) inter-planar spacing was measured as 0.366 nm.

was increased. The primary sizes of NR 1, NR 2, NR 3 and NR 4 were 528 nm, 609 nm, 754 nm and 780 nm, respectively (Table 1). Their hydrodynamic sizes were in the range of 200–300 nm, and zeta potentials were around 50 mV in water. As a control adjuvant, Alhydrogel[®] exhibited a hydrodynamic size of 259 nm and zeta potential of 22 mV in water. XRD analysis demonstrated that NRs with different lengths presented typical AIOOH peaks (Fig. 1b). Hydroxyl titration showed that there was no significant difference in the amount of hydroxyl on the surface of NRs (Figure S1 and Table 1). In contrast, BET analysis showed that their specific surface area gradually increased from 59.54 m²/g to 120.91 m²/g for NR 1 to NR 4 (Table 1).

The formation mechanism of rice-shaped NRs was further explored. At the beginning of the reaction, the initial pH was 3.4, the monomer aluminum was condensed into dimer or trimer aluminum (SI eq. 1 and Table 1). The urea was hydrolyzed to carbon dioxide and ammonia at a temperature above 90 °C, thus the pH increased rapidly to promote rapid formation of aluminum hydroxide precursors (SI eq. 2 and 3) [45,46]. After the rapid increase of pH, urea entered the slow-release process, in which it was continuously hydrolyzed to ensure the stable pH of the reaction system [47,48]. As the reaction proceeded until the pH was above 5, the aluminum hydroxide precursors underwent crystallization, and metastable AIOOH nanocrystals were formed (SI eq. 4) [49]. Due to the continu-

ous hydrolysis of urea, the pH value was increased to above 7. The isoelectric point of AIOOH NPs is 9.7 [50], thus they exhibit positive charges under weak alkaline reaction conditions, and nitrates (NO₃⁻) could be electrostatically adsorbed on the surface of AIOOH [51]. When NO₃⁻ were adsorbed onto hydroxyl-containing AIOOH surfaces such as (0 1 0) and (0 0 1), they inhibited the growth of these surfaces, which led to preferential growth of AIOOH along the direction of (1 0 0) [52]. Supersaturated metastable AIOOH nanocrystals were self-assembled into rice-shaped crystal aggregations due to this directional adsorption of NO₃⁻ and the Ostwald ripening process, thereby minimizing the surface free energy of the NPs by surface relaxation (SI eq. 5 and Fig. 2) [53–56]. The number of metastable particles was further increased due to the hydrolysis of more urea, leading to the increase of length of the NRs. The diameter of NRs remained consistent with the increase of urea-to-Al ratio during the reaction, thus further suggesting the directional growth (Table 1). The high-resolution transmission electron microscope (HRTEM) image demonstrated the occurrence of lattice fringes along particles' longitudinal direction. The corresponding inter-planar spacing was 0.366 nm that was similar with that of the (0 0 1) plane (0.369 nm) [57]. It further confirmed the orientated growth of NRs (Fig. 2b).

The crystallization and aggregation process through the interaction with interfacing atoms could promote the formation of NR

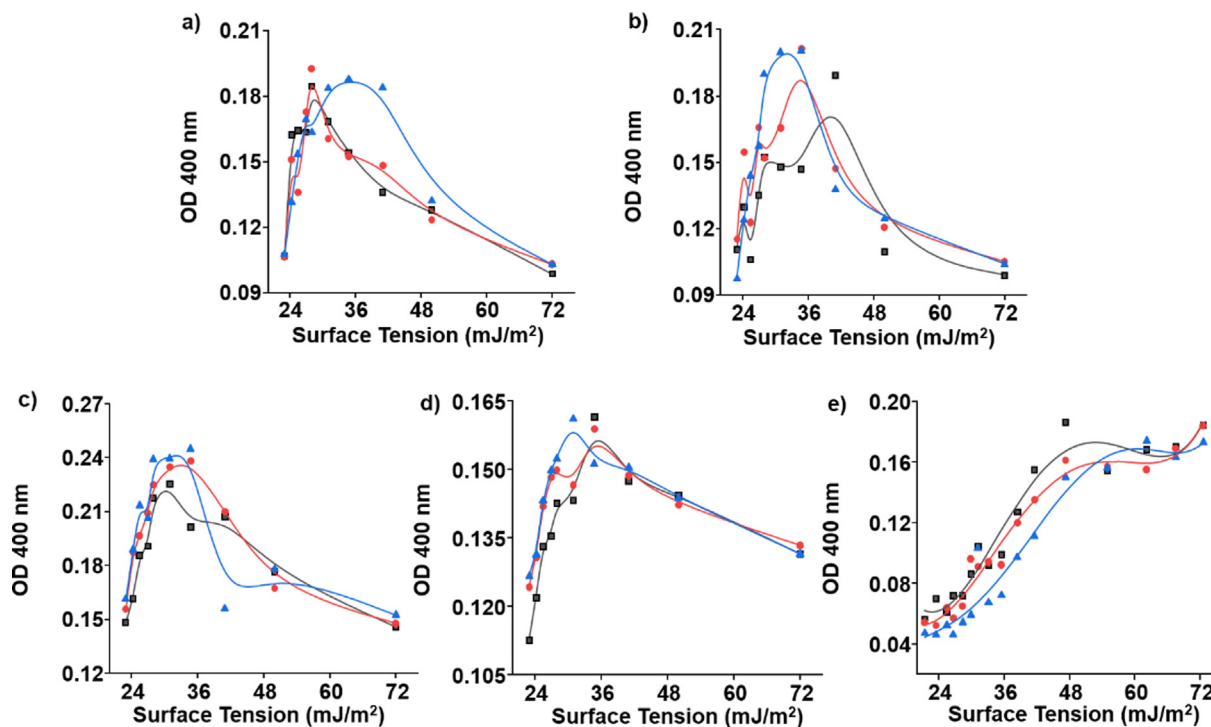


Fig. 3. Determination of the surface free energy of (a) NR 1, (b) NR 2, (c) NR 3, (d) NR 4, and (e) Alhydrogel[®] using the maximum particle dispersion (MPD) method. The optical density at 400 nm (OD 400 nm) as a function of the surface tension of the probing liquids.

Table 2

Surface free energy of NRs, disassembled NR 1 (d-NR 1), disassembled NR 4 (d-NR 4) and a commercially available adjuvant Alhydrogel[®].

Sample ID	Surface free energy (mJ/m ²)
NR 1	30.87 ± 3.07
NR 2	34.83 ± 2.65
NR 3	31.77 ± 2.03
NR 4	32.87 ± 1.55
d-NR 1	46.17 ± 0.85
d-NR 4	42.40 ± 0.94
Alhydrogel [®]	55.08 ± 3.37

aggregates to reduce the excess Gibbs free energy, and further minimize their surface free energy [58,59]. The surface free energy of NRs was determined using a maximum particle dispersion method in which the surface free energy of particles corresponds to the surface tension of probing liquid at which the particles show a maximum optical absorbance [41,60,61]. It was shown that the surface free energy of NRs (30–35 mJ/m²) was significantly lower than that of Alhydrogel[®] (55.08 mJ/m²), a commercially available adjuvant (Fig. 3 and Table 2). Furthermore, NR 1 and NR 4 were partially disassembled by probe sonication. TEM analysis showed that fragments of NRs were presenting (Figure S2a), and zeta potential measurements indicated that this disassembly process did not change their zeta potentials (Table S1). As a result, surface free energies of disassembled NR 1 (d-NR 1) and NR 4 (d-NR 4) were increased to 46.17 and 42.40 mJ/m², respectively (Figure S2b-c and Table 2). These results further confirmed that the assembled aggregation reduced the excess energy of the nanoparticles.

3.2. Assessment of suspension stability of AIOOH NRs and AIOOHs NRs-antigen complexes

In order to determine their agglomeration characteristics, NRs with different aspect ratios were dispersed in water, and their

suspension stability indexes were measured [62,63]. NRs exhibited superior stability, and their indexes maintained above 95% within 12 h. In contrast, the suspension stability of Alhydrogel[®] decreased to 85% at 12 h (Fig. 4a). The snapshots of adjuvant aqueous solutions showed that there was no obvious solid precipitation for NRs even at day 7. In contrast, the upper section of the Alhydrogel[®] suspension was completely clear and transparent (Figure S3). The suspensions of NRs were further examined in a NaCl buffer (30 mM). The indexes of NRs remained unchanged for 12 h, while that of Alhydrogel[®] decreased to 10% at 1 h (Fig. 4b). This result suggested that the higher surface free energy of Alhydrogel[®] led to the formation chaotic agglomerations. In contrast, the aggregation of NRs formed by atomic coupling provided lower surface free energy, which enabled better suspension stability [64,65]. Additionally, based on DLVO theory, the higher positive zeta potentials of NRs was another factor that may contribute to the improved suspension (Table 1) [66]. Furthermore, the suspension indexes of disassembled NR 1 (d-NR 1) and NR 4 (d-NR 4) were reduced to 85% and 75%, respectively (Figure S4 and Table 2). Analysis of rose bengal and Nile blue partitioning onto the particle surfaces demonstrated that NR 1 and disassembled NR 1 (d-NR 1) exhibited similar hydrophilicity (Figure S5). It further suggests that the surface free energy plays an important role in mediating the suspension stability.

The suspension stability of NR-antigen complexes was further assessed. Hepatitis B surface antigen (HBsAg) virus-like particles (VLPs), human papillomavirus virus (HPV) VLPs, and bovine serum albumin (BSA) were selected as model antigens. It was shown that NR-antigen complexes exhibited superior suspension stability than that of Alhydrogel[®]-antigen (Fig. 4c-e). For NR-HBsAg VLP complexes, their indexes were slowly declined to 29%, 50%, 83% and 88% for NR 1, NR 2, NR 3 and NR 4, respectively (Fig. 4c). For NRs-HPV VLPs, their indexes were 21%, 21%, 21% and 40%, respectively. For NR-BSA model, their stability indexes were all above 84%. When antigens were adsorbed by NR 4, the complexes exhibited better sta-

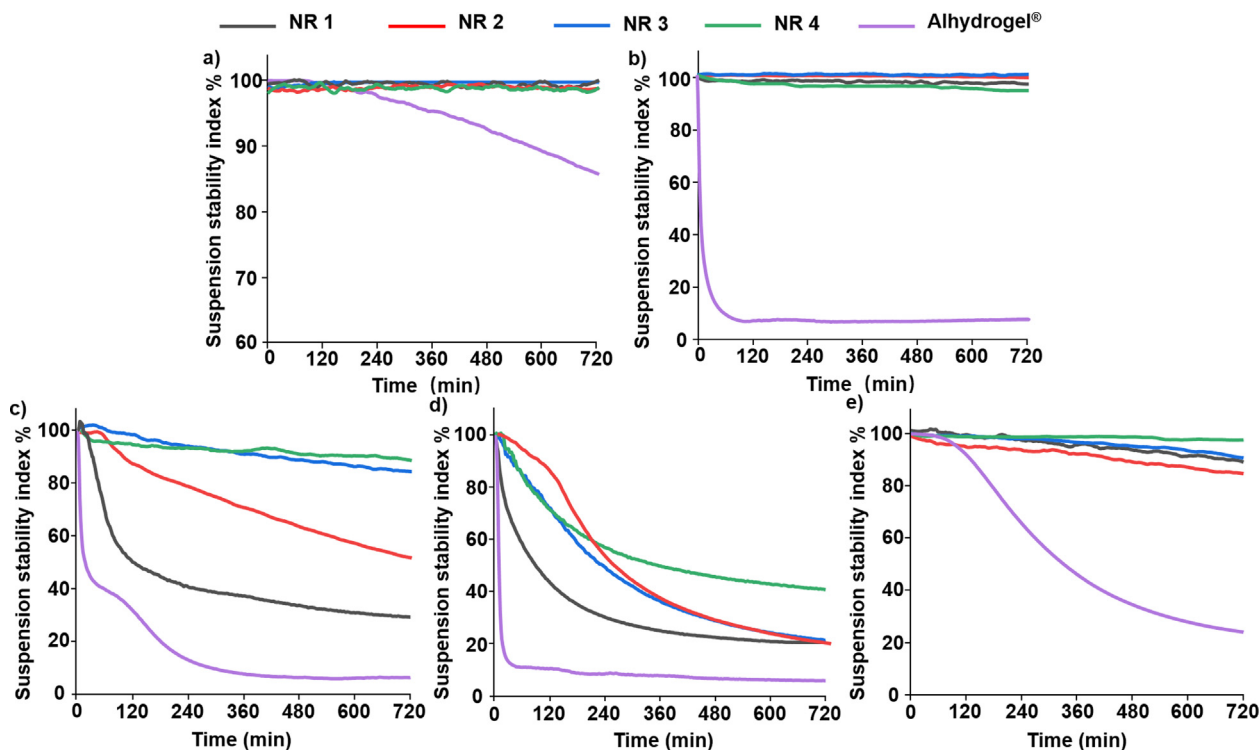


Fig. 4. Suspension stability indexes of (a) AIOOH nanoparticles in water, (b) AIOOH nanoparticles, (c) AIOOH-HBsAg VLP, (d) AIOOH-HPV VLP, and (e) AIOOH-BSA in 30 mM of NaCl within 12 h.

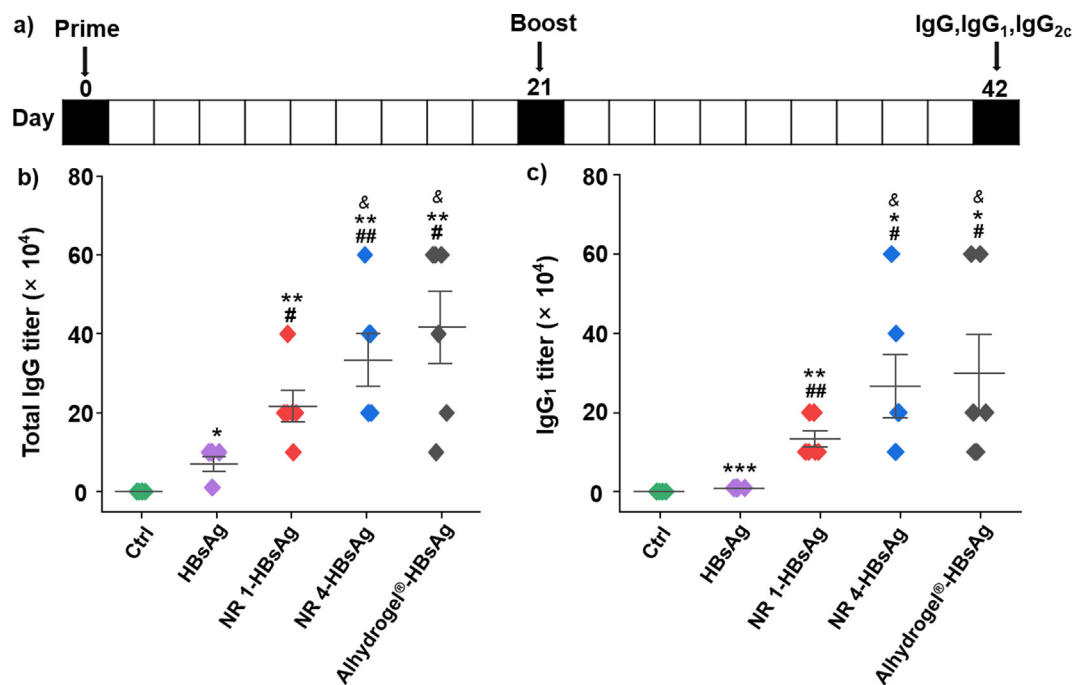


Fig. 5. (a) Schematic representation of the vaccination procedure. HBsAg specific (b) total IgG and (c) IgG₁ titers in serum were determined. **p* < 0.05, ***p* < 0.01 compared to control mice; #*p* < 0.05, ##*p* < 0.01 compared to HBsAg-treated mice; §*p* < 0.05, §§*p* < 0.01 compared to HBsAg/NR 1-treated mice.

bility than that of NR 1-antigen. Considering the fact that after absorbing the same amount of antigens, NR 4 with larger surface area could have more exposed surface area, maintaining the characteristics of lower surface free energy. It is worth noting that after adsorption of antigens, NR-antigen exhibited reduced stability, which could be related to the increased particle sizes and the

decreased surface zeta potentials (Table S2) [67,68]. In contrast, the indexes of Alhydrogel®-HBsAg VLP, Alhydrogel®-HPV and Alhydrogel®-BSA were rapidly decreased to 6%, 6% and 24%, respectively. Taken together, our designed synthesis of aggregated NRs exhibited reduced surface free energy, thus leading to superior suspension stability even after antigen adsorption.

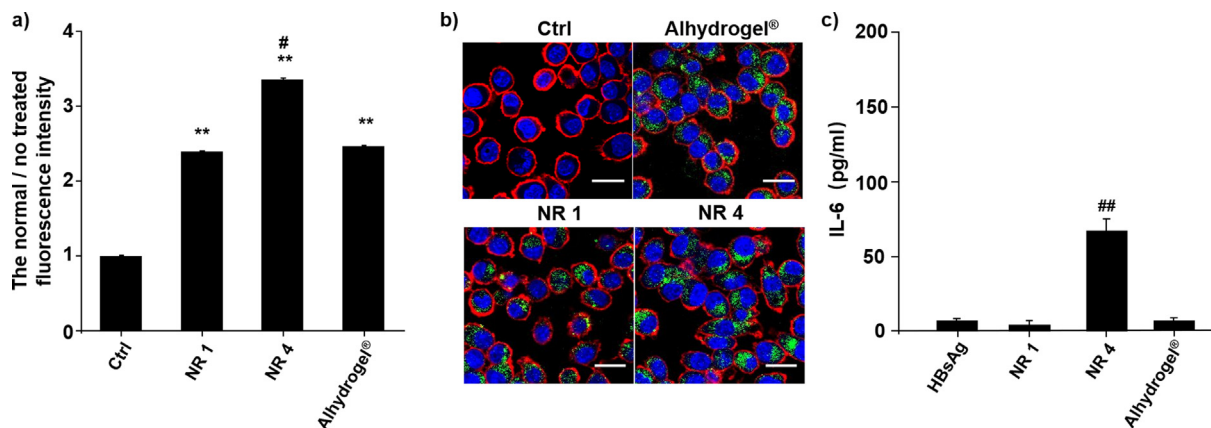


Fig. 6. (a) Flow cytometry determination of uptake of AIOOH adjuvants in J774A.1 cells. * $p < 0.05$, ** $p < 0.01$ compared to control. # $p < 0.05$, ## $p < 0.01$ compared to NR 1-treated cells. (b) Cellular uptake of AIOOH adjuvants in J774A.1 cells was determined by confocal microscopy. The nucleus was stained with Hoechst 33342 (blue), and the cell membrane was stained with WGA 594 (red). The scale bar is 20 μm . (c) IL-6 production in splenocytes was determined by ELISA. * $p < 0.05$, ## $p < 0.01$ compared to NR 1-treated cells. (For interpretation of the references to colour in this figure legend, the reader is referred to the web version of this article.)

3.3. AIOOH NRs induced enhanced humoral immune responses

Considering the superior suspension stability of the AIOOH-antigen complexes, NR 1 and NR 4 were chosen to assess their adjuvanticity *in vivo*. HBsAg was selected as the model antigen to evaluate the ability of NRs to exert the adjuvanticity. Alhydrogel® was used as a control adjuvant. Their endotoxin levels were below 0.5 EU/mL, eliminating the endotoxin contamination (Figure S6). HBsAg was pre-adsorbed on NRs before vaccination, and the adsorption study demonstrated that there was no significant difference on the adsorption capacity between NR 1 and NR 4 (Figure S7 and Table S3). Vaccine formulations, with or without NRs, were immunized intramuscularly (*i.m.*) to mice on day 0 and 21. Serum was collected on day 42 to determine the antigen-specific antibody titers (Fig. 5a). The serum biochemical analysis showed that there was no significant change in biomarkers for systematic toxicity (Table S4). NRs induced significantly higher levels of HBsAg-specific total IgG, showing the robust capability to elicit humoral immune responses. The IgG titers of HBsAg/NR 1-adjuvanted and HBsAg/NR 4-adjuvanted mice reached 2.2×10^5 and 3.3×10^5 , which were 3.1 and 4.8 folds higher than that of mice immunized with HBsAg, respectively. In addition, the HBsAg-specific IgG₁ titers showed the similar trend, with the titers of HBsAg/NR 1 and HBsAg/NR 4 being 13.3 and 26.7 folds higher than that of HBsAg-immunized mice, respectively. It should be noted that NRs with higher aspect ratio exhibited better adjuvanticity and induced comparable levels of HBsAg specific IgG and IgG₁ titers with that of Alhydrogel®-adjuvanted mice (Fig. 5b and 5c). HBsAg/NR 1 and HBsAg/NR 4 induced higher IgG_{2c} titers compared with HBsAg/Alhydrogel® (Figure S8a), however, the ratios of IgG_{2c}/IgG₁ induced by NRs and Alhydrogel® did not show significant difference compared with the one by HBsAg group (Figure S8b). Additionally, splenocytes from vaccinated mice were stimulated with HBsAg *ex vivo*, neither NRs nor Alhydrogel® induced significant IFN- γ productions (Figure S8c), which further suggested that NRs only induced Th-2 type response.

Furthermore, the potential mechanism for the better adjuvant effect of NR 4 was explored. The degree of dispersion for NR 4 was better than that of NR 1 (Table S5), and higher suspension stability could improve the degree of dispersion to increase the level of uptake by cells [69–71]. Cytotoxicity analysis showed that NRs did not exhibit cytotoxicity in J774A.1 cells (Figure S9). Cellular uptake study by quantitative flow cytometry analysis showed that J774A.1 cells took up a significant higher amount of FITC-labeled NR 4 than NR 1 (Fig. 6a), which was further verified by the confocal microscopy showing more intracellular NR4 (Fig. 6b). Enhanced cellular uptake could lead to more efficiently trigger the release

of downstream cytokines [72], which further promoted the enhanced adaptive immune responses [73]. When splenocytes from vaccinated mice were stimulated with HBsAg *ex vivo*, cells from NR 4-adjuvanted mice induced a significantly higher IL-6 production, which was agreed with the *in vitro* BMDC cytokine production profile (Fig. 6c and S10). IL-6 is a Th2-type cytokine, which plays an important role in mediating antibody responses by Alum [74,75]. Thus, NR 4's abilities to enhance adjuvant uptake and induce higher IL-6 production were correlated with their efficiency of mediating antigen-specific antibody productions [76]. Taken together, these data indicated that NRs with better suspension stability could act as effective adjuvants to enhance humoral immune responses.

4. Conclusions

To conclude, we have designed a library of rice-shaped AIOOH nanoadjuvants. The intrinsic reduction of surface free energy was achieved through controlled intraparticle aggregations in crystallization and growth processes. When NRs were formulated with model antigens, e.g., HBsAg, HPV and BSA, the NR-antigen complexes exhibited superior suspension stability. Compared with using excipient [8 77–79], this intrinsic control of surface free energy provides higher safety and efficacy for the formulation of vaccine. In a mouse HBsAg immunization model, NRs with higher aspect ratio also exhibited better adjuvanticity with enhanced humoral immune responses. The synthesis of self-assemble NRs with low surface free energy improves the suspension stability of vaccines. Results from our study can be translated to improve the suspension stability of nanomaterials in other biomedical applications.

Supporting Information

Supporting Information is available from the Journal of Colloid and Interface Science from the author.

CRedit authorship contribution statement

Shisheng Bi: Data curation, Investigation, Methodology, Validation, Writing – original draft, Writing – review & editing. **Min Li:** Methodology, Validation, Writing – review & editing. **Zhihui Liang:** Methodology, Validation, Writing – review & editing. **Guangle Li:** Methodology, Validation. **Ge Yu:** . **Jiarui Zhang:** Validation. **Chen Chen:** Validation. **Cheng Yang:** Methodology. **Changying Xue:** Methodology, Funding acquisition. **Yi Y. Zuo:** Methodology, Validation, Writing – review & editing. **Bingbing Sun:** Conceptualization,

Data curation, Funding acquisition, Resources, Project administration, Writing – review & editing.

Declaration of Competing Interest

The authors declare that they have no known competing financial interests or personal relationships that could have appeared to influence the work reported in this paper.

Acknowledgements

This work was supported by the National Natural Science Foundation of China (31870919, 21876017), Natural Science Foundation of Liaoning Province (No. XLYC1807113), Dalian Science and Technology Innovation Fund (No. 2020JJ25CY015) and Fundamental Research Funds for the Central Universities (DUT21ZD216).

Appendix A. Supplementary material

Supplementary data to this article can be found online at <https://doi.org/10.1016/j.jcis.2022.07.022>.

References

- Z. Liang, H. Zhu, X. Wang, B. Jing, Z. Li, X. Xia, H. Sun, Y. Yang, W. Zhang, L. Shi, Adjuvants for coronavirus vaccines, *Front. Immunol.* 11 (2020) 2896.
- S. Shi, H. Zhu, X. Xia, Z. Liang, X. Ma, B. Sun, Vaccine adjuvants: Understanding the structure and mechanism of adjuvanticity, *Vaccine* 37 (24) (2019) 3167–3178.
- B. Sun, T. Xia, Nanomaterial-based vaccine adjuvants, *J. Mater. Chem. B* 4 (33) (2016) 5496–5509.
- K. Muthurania, A.A. Ignatius, Z. Jin, J. Williams, S. Ohtake, Investigation of the sedimentation behavior of aluminum phosphate: influence of pH, ionic strength, and model antigens, *J. Pharm. Sci.* 104 (11) (2015) 3770–3781.
- K. Lu, Theoretical analysis of colloidal interaction energy in nanoparticle suspensions, *Ceram. Int.* 34 (6) (2008) 1353–1360.
- O.O. Kolade, W. Jin, C. Tengroth, K.D. Green, D.G. Bracewell, Shear effects on aluminum phosphate adjuvant particle properties in vaccine drug products, *J. Pharm. Sci.* 104 (2) (2015) 378–387.
- R. Nongkhlaw, P. Patra, A. Chavrasia, N. Jayabalan, S. Dubey, *Biologics: Delivery Options and Formulation Strategies, Drug Delivery Aspects*, Elsevier, 2020, pp. 115–155.
- J. Domachowski, *Vaccine Additives and Excipients*, Springer, Vaccines, 2021, pp. 49–76.
- L.A. Brito, P. Malyala, D.T. O'Hagan, Vaccine adjuvant formulations: a pharmaceutical perspective, *Seminars in immunology, Semin. Immunol.* 25 (2) (2013) 130–145.
- M.A. Malik, M.Y. Wani, M.A. Hashim, Microemulsion method: A novel route to synthesize organic and inorganic nanomaterials: 1st Nano Update, *Arabian J. Chem.* 5 (4) (2012) 397–417.
- Z. Liang, Y. Yang, G.e. Yu, H. Zhu, X. Xia, C. Chen, D. Fu, M. Li, G. Cheng, C. Xue, L. i. Shi, H. Zeng, B. Sun, Engineering aluminum hydroxyphosphate nanoparticles with well-controlled surface property to enhance humoral immune responses as vaccine adjuvants, *Biomaterials* 275 (2021) 120960.
- M. Zareei, H. Yoozbashizadeh, H.R. Madaah Hosseini, Investigating the effects of pH, surfactant and ionic strength on the stability of alumina/water nanofluids using DLVO theory, *J. Therm. Anal. Calorim.* 135 (2) (2019) 1185–1196.
- M. Larsson, A. Hill, J. Duffy, Suspension stability; why particle size, zeta potential and rheology are important, *Ann. Trans. Nordic Rheol. Soc.* 20 (2012) 6.
- P. Krishnamoorthy, Sedimentation model and analysis for differential settling of two-particle-size suspensions in the Stokes region, *Int. J. Sedim. Res.* 25 (2) (2010) 119–133.
- M. Galli, S. Sáringer, I. Szilágyi, G. Trefalt, A simple method to determine critical coagulation concentration from electrophoretic mobility, *Colloids Interfaces* 4 (2) (2020) 20.
- D. Zhou, Z. Ji, X. Jiang, D.R. Dunphy, J. Brinker, A.A. Keller, W.-C. Chin, Influence of material properties on TiO₂ nanoparticle agglomeration, *PLoS One* 8 (11) (2013) e81239.
- B.E. Rabinow, Nanosuspensions in drug delivery, *Nat. Rev. Drug Discovery* 3(9) (2004) 785–796.
- L.H. Reddy, J.L. Arias, J. Nicolas, P. Couvreur, Magnetic nanoparticles: design and characterization, toxicity and biocompatibility, pharmaceutical and biomedical applications, *Chem. Rev.* 112 (11) (2012) 5818–5878.
- M.T.H. Nutan, I.K. Reddy, General principles of suspensions, in: A.K. Kulshreshtha, O.N. Singh, G.M. Wall (Eds.), *Pharmaceutical Suspensions*, Springer New York, New York, NY, 2010, pp. 39–65.
- X.-K. Ma, N.-H. Lee, H.-J. Oh, J.-W. Kim, C.-K. Rhee, K.-S. Park, S.-J. Kim, Surface modification and characterization of highly dispersed silica nanoparticles by a cationic surfactant, *Colloids Surf. A* 358 (1–3) (2010) 172–176.
- F. Ordóñez, F. Chejne, E. Pabón, K. Cacia, Synthesis of ZrO₂ nanoparticles and effect of surfactant on dispersion and stability, *Ceram. Int.* 46 (8) (2020) 11970–11977.
- H. Heinz, C. Pramanik, O. Heinz, Y. Ding, R.K. Mishra, D. Marchon, R.J. Flatt, I. Estrela-Lopis, J. Llop, S. Moya, Nanoparticle decoration with surfactants: molecular interactions, assembly, and applications, *Surf. Sci. Rep.* 72 (1) (2017) 1–58.
- G.Y. Gor, N. Bernstein, Revisiting Bangham's law of adsorption-induced deformation: changes of surface energy and surface stress, *PCCP* 18 (14) (2016) 9788–9798.
- W. Wang, Advanced protein formulations, *Protein Sci.* 24 (7) (2015) 1031–1039.
- A. Belayneh, E. Tadese, F. Molla, Safety and biopharmaceutical challenges of excipients in off-label pediatric formulations, *Int. J. General Med.* 13 (2020) 1051.
- A. Baldwin, K.L. Kiick, Chemical conjugates for targeted degradation under reducing conditions, Google Patents (2015).
- H. Epstein, V. Berger, I. Levi, G. Eisenberg, N. Koroukhov, J. Gao, G. Golomb, Nanosuspensions of alendronate with gallium or gadolinium attenuate neointimal hyperplasia in rats, *J. Control. Release* 117 (3) (2007) 322–332.
- K. Baba, H.E. Pudavar, I. Roy, T.Y. Ohulchanskyy, Y. Chen, R.K. Pandey, P.N. Prasad, New method for delivering a hydrophobic drug for photodynamic therapy using pure nanocrystal form of the drug, *Mol. Pharm.* 4 (2) (2007) 289–297.
- N. Siedl, S.O. Baumann, M.J. Elser, O. Diwald, Particle networks from powder mixtures: generation of TiO₂-SnO₂ heterojunctions via surface charge-induced heteroaggregation, *J. Phys. Chem. C* 116 (43) (2012) 22967–22973.
- J.A. Kilner, S.J. Skinner, H.H. Brongersma, The isotope exchange depth profiling (IEDP) technique using SIMS and LEIS, *J. Solid State Electrochem.* 15 (5) (2011) 861–876.
- B. Sun, Z. Ji, Y.-P. Liao, M. Wang, X. Wang, J. Dong, C.H. Chang, R. Li, H. Zhang, A. E. Nel, T. Xia, Engineering an effective immune adjuvant by designed control of shape and crystallinity of aluminum oxyhydroxide nanoparticles, *ACS Nano* 7 (12) (2013) 10834–10849.
- Y. Hou, Y. Wang, Y. Tang, Z. Zhou, L. Tan, T. Gong, L. Zhang, X. Sun, Co-delivery of antigen and dual adjuvants by aluminum hydroxide nanoparticles for enhanced immune responses, *J. Control. Release* 326 (2020) 120–130.
- H. Jiang, Q. Wang, L. Li, Q. Zeng, H. Li, T. Gong, Z. Zhang, X. Sun, Turning the old adjuvant from gel to nanoparticles to amplify CD8⁺ T cell responses, *Adv. Sci.* 5 (1) (2018) 1700426.
- H. Li, Y. Li, J. Jiao, H.-M. Hu, Alpha-alumina nanoparticles induce efficient autophagy-dependent cross-presentation and potent antitumor response, *Nat. Nanotechnol.* 6 (10) (2011) 645–650.
- X. Li, A.M. Aldayel, Z. Cui, Aluminum hydroxide nanoparticles show a stronger vaccine adjuvant activity than traditional aluminum hydroxide microparticles, *J. Control. Release* 173 (2014) 148–157.
- X. Li, S. Hufnagel, H. Xu, S.A. Valdes, S.G. Thakkar, Z. Cui, H. Celio, Aluminum (oxy) hydroxide nanosticks synthesized in bicontinuous reverse microemulsion have potent vaccine adjuvant activity, *ACS Appl. Mater. Interfaces* 9 (27) (2017) 22893–22901.
- M. Mold, E. Shardlow, C. Exley, Toward understanding the mechanisms underlying the strong adjuvant activity of aluminium salt nanoparticles, *Ruwona TB, Xu H, Li X, Taylor AN, Shi Y, Cui Z. Vaccine* 2016; 34: 3059–67, *Vaccine* 35(8) (2017) 1101–1101.
- M.T. Orr, A.P. Khandhar, E. Seydoux, H. Liang, E. Gage, T. Mikasa, E.L. Beebe, N. D. Rintala, K.H. Persson, A. Ahniyaz, Reprogramming the adjuvant properties of aluminum oxyhydroxide with nanoparticle technology, *Npj Vaccines* 4 (1) (2019) 1–10.
- T.B. Ruwona, H. Xu, X. Li, A.N. Taylor, Y.-C. Shi, Z. Cui, Toward understanding the mechanism underlying the strong adjuvant activity of aluminum salt nanoparticles, *Vaccine* 34 (27) (2016) 3059–3067.
- B. Sun, Z. Ji, Y.-P. Liao, C.H. Chang, X. Wang, J. Ku, C. Xue, V. Mirshafiee, T. Xia, Enhanced immune adjuvant activity of aluminum oxyhydroxide nanorods through cationic surface functionalization, *ACS Appl. Mater. Interfaces* 9 (26) (2017) 21697–21705.
- Z. Cao, S.N. Tsai, Y.Y. Zuo, An optical method for quantitatively determining the surface free energy of micro- and nanoparticles, *Anal. Chem.* 91 (20) (2019) 12819–12826.
- J.C. Braun, C.E. Borba, M. Godinho, D. Perondi, J.M. Schontag, B.M. Wenzel, Phosphorus adsorption in Fe-loaded activated carbon: Two-site monolayer equilibrium model and phenomenological kinetic description, *Chem. Eng. J.* 361 (2019) 751–763.
- J. Jia, Q. Liu, T. Yang, L. Wang, G. Ma, Facile fabrication of varisized calcium carbonate microspheres as vaccine adjuvants, *J. Mater. Chem. B* 5 (8) (2017) 1611–1623.
- R. Tada, M. Ogasawara, D. Yamanaka, Y. Sakurai, Y. Negishi, H. Kiyono, N. Ohno, J. Kunisawa, Y. Aramaki, Enzymatically polymerised polyphenols prepared from various precursors potentiate antigen-specific immune responses in both mucosal and systemic compartments in mice, *PLoS One* 16 (2) (2021) e0246422.
- W. Cai, J. Yu, S. Mann, Template-free hydrothermal fabrication of hierarchically organized γ -AlOOH hollow microspheres, *Microporous Mesoporous Mater.* 122 (1–3) (2009) 42–47.

- [46] Y. Xiao, M.R. Wiesner, Characterization of surface hydrophobicity of engineered nanoparticles, *J. Hazard. Mater.* 215 (2012) 146–151.
- [47] M.M. Rao, B.R. Reddy, M. Jayalakshmi, V.S. Jaya, B. Sridhar, Hydrothermal synthesis of Mg–Al hydrotalcites by urea hydrolysis, *Mater. Res. Bull.* 40 (2) (2005) 347–359.
- [48] Z. Mohammadbagheri, A. Rahmati, P. Hoshyarmanesh, Synthesis of a novel superabsorbent with slow-release urea fertilizer using modified cellulose as a grafting agent and flexible copolymer, *Int. J. Biol. Macromol.* (2021).
- [49] J. Namieśnik, A. Rabajczyk, The speciation and physico-chemical forms of metals in surface waters and sediments, *Chem. Speciat. Bioavailab.* 22 (1) (2010) 1–24.
- [50] I.S. Martakov, O.G. Shevchenko, Synthesis and enhanced antioxidant and membrane-protective activity of curcumin@ ALOOH nanoparticles, *J. Inorg. Biochem.* 210 (2020) 111168.
- [51] I. Martakov, O. Shevchenko, M. Torlopov, E.Y. Gerasimov, P. Sitnikov, Formation of gallic acid layer on γ -ALOOH nanoparticles surface and their antioxidant and membrane-protective activity, *J. Inorg. Biochem.* 199 (2019) 110782.
- [52] W. Cai, J. Yu, M. Jaroniec, Template-free synthesis of hierarchical spindle-like γ -Al₂O₃ materials and their adsorption affinity towards organic and inorganic pollutants in water, *J. Mater. Chem.* 20 (22) (2010) 4587–4594.
- [53] X. Wang, L. Xu, K. Song, R. Yang, L. Jia, X. Guo, X. Jing, J. Wang, Synthesis of MnCo₂O₄@ MnCo₂S₄ core/shell micro-nanostructures on Ni foam for high performance asymmetric supercapacitors, *Colloids Surf., A* 570 (2019) 73–80.
- [54] M.R. Chowdhury, Solvent dependent growth of one-dimensional crystalline β -FeOOH nanorods, Unpublished DTech: Chemical Engineering thesis, Cape Peninsula University of Technology, Cape Town, South Africa, 2014.
- [55] A. Baldan, Review progress in Ostwald ripening theories and their applications to nickel-base superalloys Part I: Ostwald ripening theories, *J. Mater. Sci.* 37 (11) (2002) 2171–2202.
- [56] K. Tanaka, A. Takahara, T. Kajiyama, Rheological analysis of surface relaxation process of monodisperse polystyrene films, *Macromolecules* 33 (20) (2000) 7588–7593.
- [57] T. He, L. Xiang, W. Zhu, S. Zhu, H₂SO₄-assisted hydrothermal preparation of γ -ALOOH nanorods, *Mater. Lett.* 62 (17–18) (2008) 2939–2942.
- [58] I.A. Mudunkotuwa, V.H. Grassian, The devil is in the details (or the surface): impact of surface structure and surface energetics on understanding the behavior of nanomaterials in the environment, *J. Environ. Monit.* 13 (5) (2011) 1135–1144.
- [59] L. Xu, H.-W. Liang, Y. Yang, S.-H. Yu, Stability and reactivity: positive and negative aspects for nanoparticle processing, *Chem. Rev.* 118 (7) (2018) 3209–3250.
- [60] G. Li, Z. Cao, K.K. Ho, Y.Y. Zuo, Quantitative Determination of the Hydrophobicity of Nanoparticles, *Anal. Chem.* 94 (4) (2022) 2078–2086.
- [61] G. Li, K.K. Ho, Y.Y. Zuo, Relative dye adsorption method for determining the hydrophobicity of nanoparticles, *J. Phys. Chem. C* 126 (1) (2021) 832–837.
- [62] T. Kim, C.-H. Lee, S.-W. Joo, K. Lee, Kinetics of gold nanoparticle aggregation: experiments and modeling, *J. Colloid Interface Sci.* 318 (2) (2008) 238–243.
- [63] R. Pamies, J.G.H. Cifre, V.F. Espín, M. Collado-González, F.G.D. Baños, J.G. de la Torre, Aggregation behaviour of gold nanoparticles in saline aqueous media, *J. Nanopart. Res.* 16 (4) (2014) 1–11.
- [64] K.S. Hayden, K. Park, J.S. Curtis, Effect of particle characteristics on particle pickup velocity, *Powder Technol.* 131 (1) (2003) 7–14.
- [65] S.U. Ilyas, R. Pendyala, N. Marneni, Preparation, sedimentation, and agglomeration of nanofluids, *Chem. Eng. Technol.* 37 (12) (2014) 2011–2021.
- [66] J.A.A. Júnior, J.B. Baldo, The behavior of zeta potential of silica suspensions, *New J. Glass Ceramics* 4 (02) (2014) 29.
- [67] P. Bihari, M. Vippola, S. Schultes, M. Praetner, A.G. Khandoga, C.A. Reichel, C. Coester, T. Tuomi, M. Rehberg, F. Krombach, Optimized dispersion of nanoparticles for biological in vitro and in vivo studies, *Part. Fibre Toxicol.* 5 (1) (2008) 1–14.
- [68] A. Langford, T. Horwitz, E. Adu-Gyamfi, C. Wiley, E. Holding, D. Zimmermann, A.A. Ignatius, S. Ohtake, Impact of Formulation and Suspension Properties on Redispersion of Aluminum-Adjuvanted Vaccines, *J. Pharm. Sci.* 109 (4) (2020) 1460–1466.
- [69] Y. Luo, Z. Teng, Y. Li, Q. Wang, Solid lipid nanoparticles for oral drug delivery: Chitosan coating improves stability, controlled delivery, mucoadhesion and cellular uptake, *Carbohydr. Polym.* 122 (2015) 221–229.
- [70] A. Albanese, W.C. Chan, Effect of gold nanoparticle aggregation on cell uptake and toxicity, *ACS Nano* 5 (7) (2011) 5478–5489.
- [71] Y.T. Yang, C.T. Chen, J.C. Yang, T. Tsai, Spray-dried microparticles containing polymeric micelles encapsulating hematoporphyrin, *AAPS J.* 12 (2) (2010) 138–146.
- [72] C. Li, X. Zhang, Q. Chen, J. Zhang, W. Li, H. Hu, X. Zhao, M. Qiao, D. Chen, Synthetic polymeric mixed micelles targeting lymph nodes trigger enhanced cellular and humoral immune responses, *ACS Appl. Mater. Interfaces* 10 (3) (2018) 2874–2889.
- [73] J.R. Adams, S.K. Mallapragada, Enhancing the immune response through next generation polymeric vaccine adjuvants, *Technology* 2 (01) (2014) 1–12.
- [74] B. Sun, X. Wang, Z. Ji, R. Li, T. Xia, NLRP3 inflammasome activation induced by engineered nanomaterials, *Small* 9 (9–10) (2013) 1595–1607.
- [75] B. Liang, D.B. Gardner, D.E. Griswold, P.J. Bugelski, X.Y.R. Song, Antiinterleukin-6 monoclonal antibody inhibits autoimmune responses in a murine model of systemic lupus erythematosus, *Immunology* 119 (3) (2006) 296–305.
- [76] Z. Liang, X. Wang, G. Yu, M. Li, S. Shi, H. Bao, C. Chen, D. Fu, W. Ma, C. Xue, Mechanistic understanding of the aspect ratio-dependent adjuvanticity of engineered aluminum oxyhydroxide nanorods in prophylactic vaccines, *Nano Today* 43 (2022) 101445.
- [77] Q. Sun, Z. Li, S. Li, L. Jiang, J. Wang, P. Wang, Utilization of surfactant-stabilized foam for enhanced oil recovery by adding nanoparticles, *Energy Fuels* 28 (4) (2014) 2384–2394.
- [78] T. Clapp, P. Siebert, D. Chen, L.J. Braun, Vaccines with aluminum-containing adjuvants: optimizing vaccine efficacy and thermal stability, *J. Pharm. Sci.* 100 (2) (2011) 388–401.
- [79] A.C. Silva, M.J. Carrondo, P.M. Alves, Strategies for improved stability of peste des petits ruminants vaccine, *Vaccine* 29 (31) (2011) 4983–4991.